Self-aggregated dinuclear lanthanide(III) complexes as potential bimodal probes for magnetic resonance and optical imaging[i]

Martín Regueiro-Figueroa[a], Aline Nonat[b], Gabriele A. Rolla[c], David Esteban-Gómez[a], Andrés de Blas[a], Teresa Rodríguez-Blas[a], Loïc J. Charbonnière[b*], Mauro Botta[c], Carlos Platas-Iglesias[a†]

[a] Departamento de Química Fundamental, Universidade da Coruña, Campus da Zapateira, Rúa da Fraga 10, 15008 A Coruña (Spain)

[b] Laboratoire d'Ingénierie Moléculaire Appliquée à l'Analyse, IPHC, UMR 7178 CNRS/UdS, ECPM Bâtiment R1N0, 25 rue Becquerel, 67087 Strasbourg Cedex (France)

[c] Dipartimento di Scienze e Innovazione Tecnologica, Università del Piemonte Orientale "A. Avogadro", Viale T. Michel 11, 15121 Alessandria (Italy)

Chemistry – A European Journal, volume 19, issue 35, pages 11696–11706, 26 August 2013
Received 01 April 2013, version of record online 11 July 2013, issue online 19 August 2013

Abstract

Homodinuclear lanthanide complexes (Ln=La, Eu, Gd, Tb, Yb and Lu) derived from a bis-macrocyclic ligand featuring two 2,2′,2″-(1,4,7,10-tetraazacyclododecane-1,4,7-triyl)triacetic acid chelating sites linked by a 2,6-bis(pyrazol-1-yl)pyridine spacer (H_2L^3) were prepared and characterized. Luminescence lifetime measurements recorded on solutions of the Eu^{III} and Tb^{III} complexes indicate the presence of one inner-sphere water molecule coordinated to each metal ion in these complexes. The overall luminescence quantum yields were determined ($Ø_{H_2O}$=0.01 for $[Eu_2(L^3)]$ and 0.50 for $[Tb_2(L^3)]$ in 0.01 M TRIS/HCl, pH 7.4; TRIS=tris(hydroxymethyl)aminomethane), pointing to an effective sensitization of the metal ion by the bispyrazolylpyridyl unit of the ligand, especially with Tb. The nuclear magnetic relaxation dispersion (NMRD) profiles recorded for $[Gd_2(L^3)]$ are characteristic of slowly tumbling systems, showing a low-field plateau and a broad maximum around 30 MHz. This suggests the occurrence of aggregation of the complexes giving rise to slowly rotating species. A similar behavior is observed for the analogous Gd^{III} complex containing a 4,4′-dimethyl-2,2′-bipyridyl spacer ($[Gd_2(L^1)]$). The relaxivity of $[Gd_2(L^3)]$ recorded at 0.5 T and 298 K (pH 6.9) amounts to 13.7 $mM^{-1}\,s^{-1}$. The formation of aggregates has been confirmed by dynamic light scattering (DLS) experiments, which provided mean particle sizes of 114 and 38 nm for $[Gd_2(L^1)]$ and $[Gd_2(L^3)]$, respectively. TEM images of $[Gd_2(L^3)]$ indicate the formation of nearly

* l.charbonn@unistra.fr
† carlos.platas.iglesias@udc.es

spherical nanosized aggregates with a mean diameter of about 41 nm, together with some nonspherical particles with larger size.

Keywords: europium; gadolinium; lanthanides; luminescence; magnetic resonance imaging

Introduction

Lanthanide(III) complexes with poly(aminocarboxylate) ligands are gaining increasing interest due to their successful application in different imaging modalities. For instance, luminescent lanthanide complexes present unique photophysical properties that find applications in fields such as biomedical analyses and imaging,[1] while gadolinium complexes are currently used as contrast agents in magnetic resonance imaging (MRI).[2,3] Lanthanide(III) complexes for application in these fields require stable complexation of the metal ion with adequate ligands to prevent the release of the toxic free-metal ion.[4,5] Poly(aminocarboxylate) ligands based on either linear or macrocyclic frameworks are often used for this purpose, while macrobicyclic ligands have also been successfully used mostly for in vitro bioanalytical applications.[6]

A current challenge in the field of molecular imaging is the design of bimodal probes that could combine the advantages of two different imaging modalities.[7,8] For instance, bimodal probes for MRI and optical imaging are expected to couple the high sensitivity of luminescence and the high spatial resolution of MRI.[9] A lanthanide-based bimodal probe must contain suitable chromophoric units to provide an efficient energy transfer to populate the Ln^{III} ion excited state (antenna effect).[10] Moreover, the ligand must provide an adequate protection of the metal ion from the environment to minimize the quenching effect of O–H oscillators of coordinated water molecules, which provide an efficient pathway for the radiationless deactivation of the Ln^{III}-centered excited states.[11] Additionally, stable Gd^{III}chelates for application as MRI contrast agents should contain at least one water molecule coordinated to the metal ion that can rapidly exchange with the bulk water of the body, which imparts an efficient mechanism for the longitudinal and transverse relaxation enhancement ($1/T_1$ and $1/T_2$) of water protons.[12,13] The efficiency of a contrast agent in vitro is measured in terms of its relaxivity (r_{1p}),[14] which is defined as the relaxation-rate enhancement of water protons per mM concentration of metal ion. Interestingly, it has been shown that certain Ln^{III} complexes containing one or two inner-sphere water molecules present relatively high luminescence quantum yields of the Ln^{III} centered luminescence and high relaxivities.[15]

Most of the Ln^{III}-based systems proposed as bimodal probes (MRI/optical imaging) are based on small coordination compounds,[15–17] but an interesting alternative was found in the development of several examples of Gd^{III}-loaded nanoparticles containing organic dyes as dual probes.[18] Nanoparticles loaded with Gd^{III} and luminescent units provide some advantages over small complexes, as they allow to deliver a high payload of Gd^{III} to the target tissue, thereby overcoming the intrinsic low sensitivity of MRI. Besides, dual nanoprobes responsive in MRI and optical imaging ensure identical biodistribution in the two imaging modalities.

We have recently shown that homodinuclear Ln^{III} complexes containing two 2,2′,2″-(1,4,7,10-tetraazacyclododecane-1,4,7-triyl)triacetic acid (DO3A) units linked by 4,4′-dimethyl-2,2′-bipyridyl ($[Ln_2(L^1)]$, Scheme 1) or 6,6′-dimethyl-2,2′-bipyridyl ($[Ln_2(L^2)]$) units provide an efficient sensitization of both Eu^{III} and Tb^{III}.[19,20] Additionally, the bipyridyl coordination site of $[Ln_2(L^1)]$ complexes was used to introduce $\{Ru(bpy)_2\}$ (bpy=2,2′-bipyridine) and $\{Re(CO)_3Cl\}$ moieties, leading to the formation of heterometallic d–f_2 complexes that provide an efficient sensitization of the NIR emission of Nd^{III} and Yb^{III} in aqueous solutions. We and others have also shown that the bispyrazolylpyridyl chromophore incorporated to polyaminocarboxylate ligands can act as an efficient antenna to sensitize the luminescence of different Ln^{III} ions that emit both in the visible and NIR regions.[21–23] Herein we report the results of a study on

$[Ln_2(L^3)]$ systems in which two DO3A units are linked by a bispyrazolylpyridyl unit. The photophysical properties of the Eu^{III} and Tb^{III} complexes have been investigated in detail, and luminescence lifetime measurements have been used to determine their hydration numbers. Nuclear magnetic relaxation dispersion (NMRD) investigations on the $[Gd_2(L^3)]$ complex and the $[Gd_2(L^1)]$ and $[Gd_2(L^2)]$ analogues were performed in order to assess their ^1H relaxation enhancement abilities and to gain insight into the molecular parameters governing the relaxivity. The $[Gd_2(L^1)]$ and $[Gd_2(L^3)]$ complexes form nanosized aggregates that were characterized by dynamic light scattering (DLS) and transmission electron microscopy (TEM).

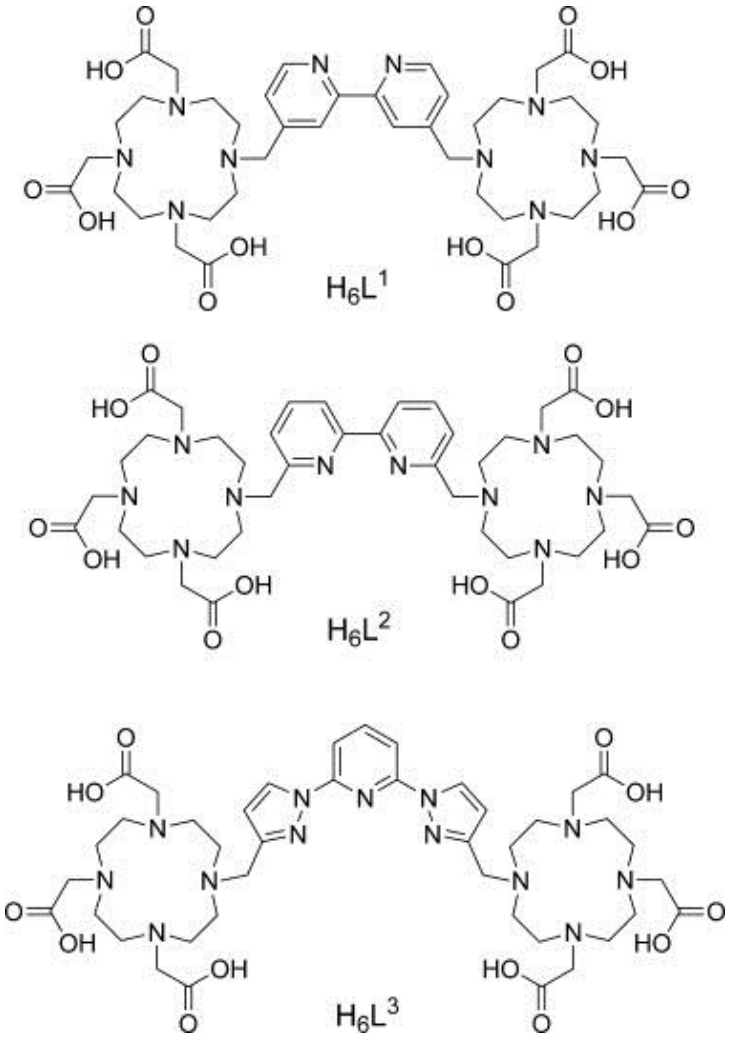

Scheme 1. Ligands discussed in the present work.

Results and discussion

Synthesis and characterization of the ligand L^3 and the corresponding Ln^{III} complexes

The synthetic strategy used for the preparation of H_6L^3 and its Ln^{III} complexes is shown in Scheme 2. 2,6-Bis(3-bromomethyl-1-pyrazolyl)pyridine (**1**) was prepared by following the published procedure.[23] *N*-Alkylation of DO3A(*t*BuO)$_3$[24] with **1** in refluxing acetonitrile in the presence of Na_2CO_3 gave compound **2** in 78 % yield. Full deprotection of the *tert*-butyl esters of **2** was cleanly achieved with a

CF_3COOH/H_2O (1:1) mixture to give the desired ligand as the hexatrifluoroacetate salt (81 % yield). Subsequent reaction of $H_6L^3 \cdot 6CF_3COOH \cdot 5H_2O$ with lanthanide triflates in the presence of an excess of triethylamine resulted in the formation of compounds of formula $[Ln_2(L^3)] \cdot 2\,H_2O$ (Ln=La, Eu, Gd, Tb, Yb or Lu), which were isolated in excellent yields (87-91 %). The high-resolution mass spectra (ESI^+) show peaks corresponding to the $[Ln_2(L^3+2\,H)]^{2+}$, $[Ln_2(L^3+2Na)]^{2+}$, $[Ln_2(L^3+H)]^+$ or $[Ln_2(L^3+Na)]^+$ entities (Figures S1–S6 in the Supporting Information), which confirms the formation of the desired binuclear neutral complexes.

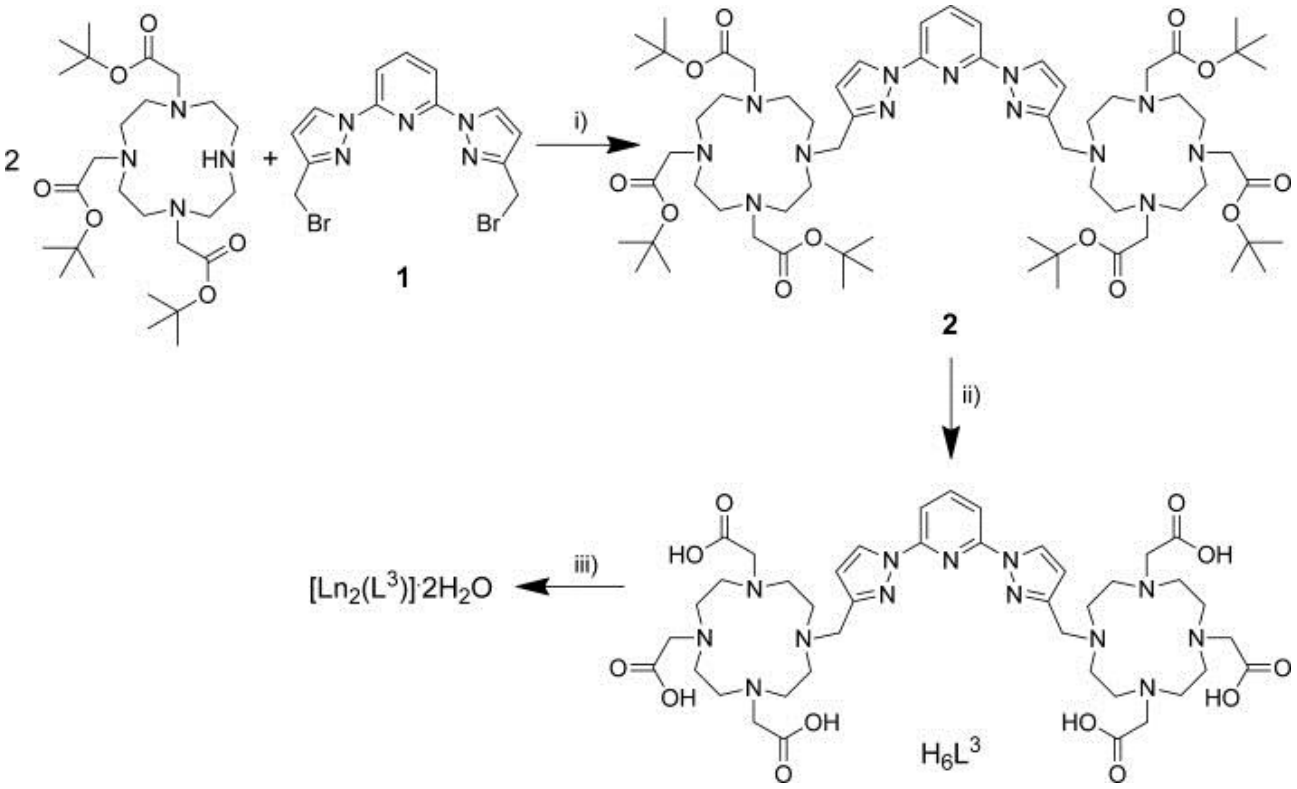

Scheme 2. i) Na_2CO_3, CH_3CN, Δ; ii) CF_3COOH/H_2O (1:1), Δ; iii) $Ln(CF_3SO_3)_3$, Et_3N, 2-propanol, Δ.

The ^1H spectrum of the diamagnetic $[Lu_2(L^3)]$ complex recorded in D_2O (500 MHz, 298 K, pD 7.0) shows four broad signals in the range 6.6–8.5 ppm, together with extremely broad signals in the region 2.6–4.3 ppm typical of Ln^{III} complexes with *N*-alkylated DO3A derivatives undergoing intramolecular dynamic exchange processes (Figure S9 in the Supporting Information).[25] However, the presence of four signals in the aromatic region points to an effective C_2 symmetry of the complex in solution, suggesting that the two Ln^{III} ions present identical coordination environments. A similar situation was previously observed for the complexes of L^1,[20] in contrast to those of L^2,[19] which present a C_1 symmetry in solution with two different coordination environments around the two Ln^{III} ions. The ^1H NMR spectrum of the paramagnetic $[Yb_2(L^3)]$ complex (300 MHz, 298 K, pD 7.0) also shows very broad signals due to exchange phenomena (Figure S10 in the Supporting Information). The pseudo-axial protons on the cyclen rings are observed as a very broad signal at 90 ppm. The chemical shift of this signal is characteristic of square-antiprismatic coordination geometries around the two metal ions by comparison with related compounds.[26]

Photophysical properties of the $[Ln_2(L^3)]$ complexes (Ln=Eu or Tb)

The photophysical properties of the Eu^{III} and Tb^{III} complexes of L^3 are summarized in Table 1. The UV/Vis absorption spectra of the $[Eu_2(L^3)]$ and $[Tb_2(L^3)]$ complexes in 0.01 M TRIS-buffered aqueous solutions (pH

7.4; TRIS=tris(hydroxymethyl)aminomethane) are presented in Figure 1. Both spectra display two strong absorption bands: one centered at 245 nm (ε=15 000 and 18 000 M^{-1} cm^{-1} for [$Eu_2(L^3)$] and [$Tb_2(L^3)$], respectively), and the other at 295 nm (ε=9770 and 11 970 M^{-1} cm^{-1} for [$Eu_2(L^3)$] and [$Tb_2(L^3)$], respectively). Both are characteristic of $\pi\rightarrow\pi^*$ transitions centered on the aromatic moieties.[21,23] Interestingly, it can be noted that the maxima of the low-energy absorption bands (295 nm) correspond to a bis(pyrazolyl)pyridine system in a *trans–trans* conformation, as the isomerization to the *cis–cis* conformation results in a bathochromic shift to about 315 nm.[21] This indicates that the central pyridine nitrogen atom of the aromatic tridentate unit is not coordinated to the Ln^{III} ion.

Table 1. Selected photophysical data for [$Ln_2(L^1)$], [$Ln_2(L^2)$], and [$Ln_2(L^3)$] complexes (Ln=Eu or Tb) in aqueous solutions.

	$\emptyset_{H_2O}$	$\emptyset_{D_2O}$ [c]	$\emptyset_{Ln}^{Ln}$	τ_{H_2O} [µs]	τ_{D_2O} [µs] [c]	q [f]
[$Eu_2(L^1)$]	0.084 [a]	–	0.13 [a]	560 [a]	1680	0.8
[$Tb_2(L^1)$]	0.25 [a]	–	–	1440 [a]	2540	1.3
[$Eu_2(L^2)$]	0.07 [b]	0.16	0.16 [b]	1210 [b,d]	1900 [d]	0.1 [d]
				440 [b,e]	ca. 1800 [e]	1.8 [e]
[$Tb_2(L^2)$]	0.51 [b]	0.57	–	2048 [b]	3180	0.6
[$Eu_2(L^3)$]	0.01 [b]	0.05	0.11 [b]	624 [b]	1879	1.0
[$Tb_2(L^3)$]	0.50 [b]	0.99	–	1858 [b]	3952	1.1

[a] TRIS/HCl, pH 7.4, 0.1 M. [b] TRIS/HCl, pH 7.4, 0.01 M. [c] D_2O, pD 7.4. [d] Site I. [e] Site II. [f] According to ref. 28. Estimated errors: ±10 % on lifetimes, ±15 % on quantum yields.

Upon excitation into the absorption band in the UV/Vis domain, the complexes display emission patterns characteristic of the $^5D_0\rightarrow{}^7F_J$ (J=0-4) and $^5D_4\rightarrow{}^7F_J$ (J=6-3) transitions of the Eu^{III} and Tb^{III} ions, respectively (Figure 1).[27] In both cases, no residual fluorescence of the ligand could be observed. Moreover, the excitation spectra recorded upon metal-centered emission are very similar to the corresponding absorption spectra, which strongly suggest an efficient ligand-to-metal energy transfer (Figure 1).

A detailed analysis of the Eu^{III} emission spectrum (Figure 1) reveals the presence of one sharp component centered at 579.0 nm corresponding to the $^5D_0\rightarrow{}^7F_0$ transition, which is indicative of the presence of a single species in solution. The spectral region corresponding to the $^5D_0\rightarrow{}^7F_1$ transitions displays three emission lines centered at 588.7, 591.4, and 598.0 nm, characteristic of species with low symmetry.

The average hydration states of [$Eu_2(L^3)$] and [$Tb_2(L^3)$] were determined thanks to their luminescence lifetimes in H_2O and D_2O[28] upon emission at 613 and 541 nm, respectively. The emission decays could be fitted to mono-exponential decays and the corresponding lifetimes (Table 1) are in agreement with the formation of mono-hydrated species (q=1.0 and 1.1 for the Eu and Tb complexes, respectively).[28] The lifetimes measured for [$Eu_2(L^3)$] and [$Tb_2(L^3)$] are slightly longer than those previously measured for L^1 analogues with the bridging methylene groups in the 4- and 4′-positions of the bipyridyl spacer. The sensitized emission quantum yields of [$Eu_2(L^3)$] ($\emptyset_{H_2O}$=0.01) and [$Tb_2(L^3)$] ($\emptyset_{H_2O}$=0.5) were determined in 0.01 M TRIS/HCl-buffered aqueous solutions (pH 7.4) by using [$Ru(bpy)_3$]Cl_2 ($\emptyset_{H_2O}$=0.04)[29] in non-degassed water as a reference for Eu^{III} and Rhodamine 6G ($\emptyset_{H_2O}$=0.76)[30] in water for Tb^{III}. These values indicate a better emission quantum yield of the Tb^{III} center when excited through the bispyrazolylpyridyl unit of L^3 than when excited by the bipyridine chromophore of L^1 substituted in the 4- and 4′-positions ($\emptyset_{H_2O}$=0.25 for [$Tb_2(L^1)$]). The overall emission quantum yields of [$Eu_2(L^3)$] and [$Tb_2(L^3)$] have also been

measured in D_2O and they amount to $\emptyset_{D_2O}$=0.05 and 0.99, respectively. The emission quantum yield of [$Tb_2(L^3)$] is virtually identical to that determined for [$Tb_2(L^2)$], in which the bipyridyl unit coordinates to one of the Tb^{III} ions.[19] The quantum yields determined in D_2O clearly indicate that the losses in luminescence are essentially due to quenching by water molecules in the case of [$Tb_2(L^3)$], whereas they can be in part attributed to intramolecular Tb to Tb energy transfer in the case of L^2.[19]

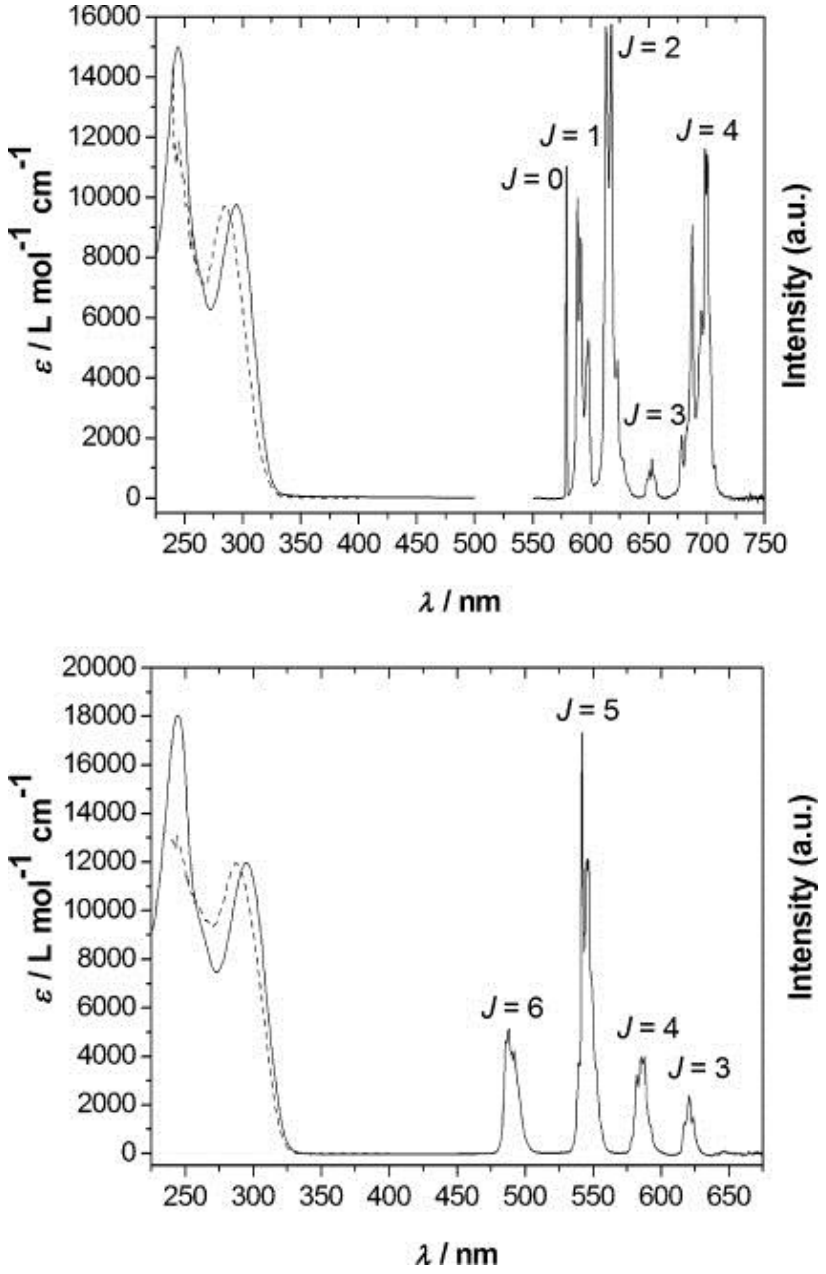

Figure 1. UV/Vis absorption spectra, excitation spectra (dotted lines, Ln=Eu, λ_{em}=614 nm; Ln=Tb, λ_{em}=541 nm) and high resolution emission spectra (λ_{ex}=287 nm) recorded for the complexes [$Eu_2(L^3)$] (top) and [$Tb_2(L^3)$] (bottom) in 0.01 M TRIS/HCl buffered aqueous solutions (pH 7.4, 5×10^{-5} M).

Relaxometric characterization of [$Gd_2(L^1)$], [$Gd_2(L^2)$], and [$Gd_2(L^3)$] complexes

The effectiveness of a metal-based MRI probe in increasing the longitudinal relaxation rate of water protons is defined by the parameter r_{1p} that, as mentioned above, describes the observed enhancement normalized to

a one mM concentration of the paramagnetic ion and is dependent on temperature and applied magnetic field strength. The increase of the proton longitudinal relaxation rate of the water proton nuclei is predominantly the result of the modulation of the dipolar interaction between the electron spin of the paramagnetic metal ion and the nuclear magnetic moment of coordinated water molecules. This time modulation depends on four correlation times: the rotational correlation time (τ_R), the longitudinal (T_{1e}) and transverse (T_{2e}) electron relaxation times, and the mean residence lifetime of water protons in the inner coordination sphere (τ_M). Relaxivity also depends on the number of bound water molecules (q) and their distance (r_{Gd-H}) from the metal center. Additionally, there is a contribution to relaxivity arising from solvent molecules diffusing in the vicinity of the paramagnetic complex (outer-sphere mechanism), which depends on the relative diffusion coefficient of solute and solvent molecules (D) and their distance of closest approach (a).[2]

The r_{1p} value of [$Gd_2(L^1)$] recorded at 0.5 T and 298 K (Figure 2) is relatively high (ca. 10.2 $mM^{-1}\,s^{-1}$), and remains constant over a broad pH range (pH 5.0–11.5). The relaxivity of [$Gd_2(L^3)$] recorded at pH 10.0 is even higher (13.0 $mM^{-1}\,s^{-1}$), and increases slightly as the pH is lowered, assuming a value of 13.7 $mM^{-1}\,s^{-1}$ at pH 6.9. At lower pH values r_{1p} decreases sharply due to precipitation of the complex. In the case of [$Gd_2(L^2)$] the relaxivity at 0.5 T and 298 K is considerably lower than for the corresponding complexes of L^1 and L^3. It assumes a value of about 7.1 $mM^{-1}\,s^{-1}$ in the pH range 4.4–7.9, and then decreases reaching a value of 5.4 $mM^{-1}\,s^{-1}$ at pH 11.5. The ^1H NMR spectra of the Yb^{III} and Lu^{III} complexes of L^2 remain unchanged over the pH range 6–11, which indicates that the drop in relaxivity observed for [$Gd_2(L^2)$] is not associated with a drastic change of the coordination environment of the metal ions. Interestingly, previous spectroscopic studies on the Eu and Tb complexes of L^2have shown this ligand to be the only example for which the two cations are not in the same environment. It was found that one of the two cations is fully saturated by the donor atoms of the ligand, while the second metal ion is coordinated to two water molecules.[19] A drop of r_{1p} has been observed previously for different Gd^{III} complexes with heptadentate macrocyclic ligands, and it was attributed to the displacement of the coordinated water molecules by formation of ternary complexes with the carbonate present in the aerated aqueous solution.[31,32]

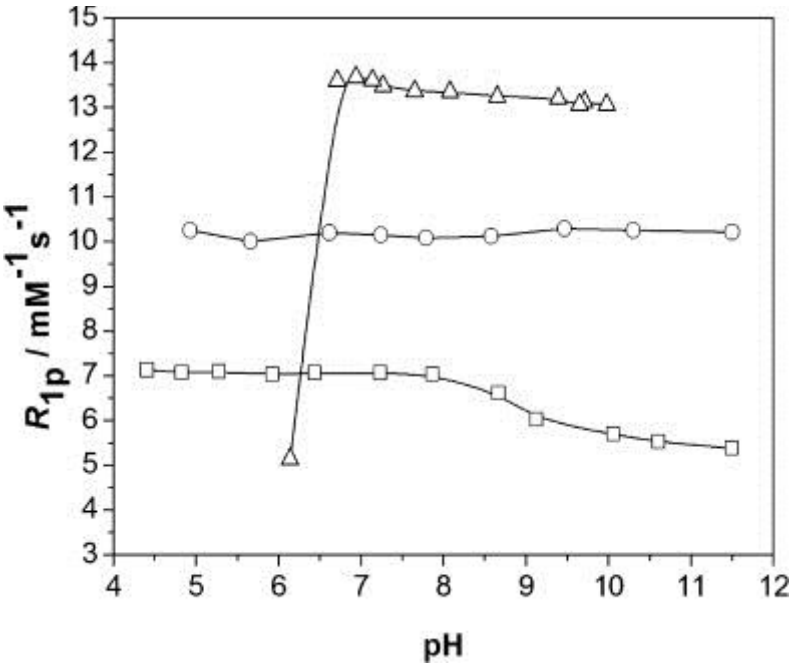

Figure 2. Plot of the relaxivity (0.5 T; 298 K) of the Gd^{III} complexes investigated in this work as a function of pH. The solid lines are simply a guide for the eye. [$Gd_2(L^1)$]: ○; [$Gd_2(L^2)$]: □; [$Gd_2(L^3)$]: ▵.

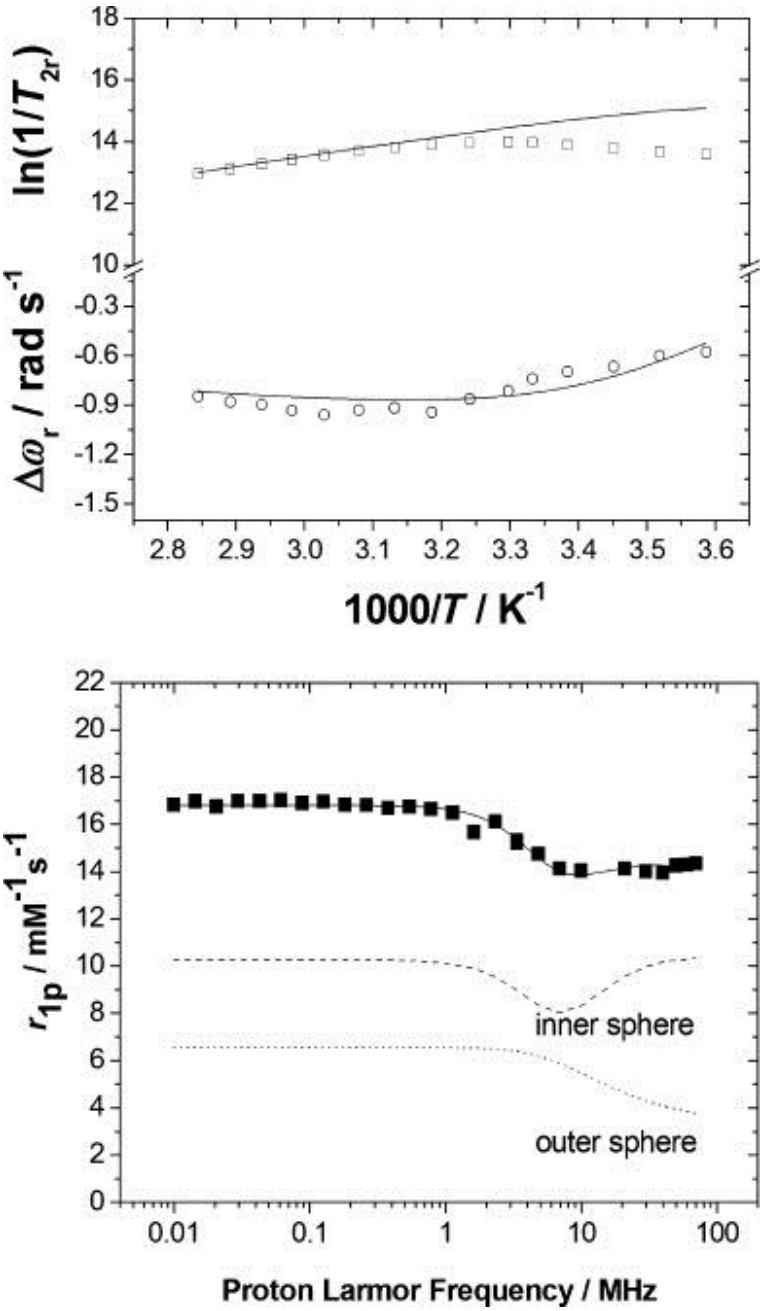

Figure 3. Top: Reduced transverse ^{17}O relaxation rates (squares) and ^{17}O chemical shifts (circles) of a $[Gd_2(L^2)]$ solution (19 mM) at 11.75 T and neutral pH. Bottom: NMRD profile recorded for $[Gd_2(L^2)]$ (7.7 mM) at 298 K and outer- and inner-sphere contributions obtained from the analysis of the data. Relaxivities are expressed per molecule (instead of per mM concentration of Gd^{III}) due to the presence of two metal ions with different coordination environments (see text). The solid lines represent the fit of the data as described in the text.

Nuclear magnetic relaxation dispersion (NMRD) profiles of aqueous solutions of $[Gd_2(L^1)]$, $[Gd_2(L^2)]$, and $[Gd_2(L^3)]$ were measured at 283, 298, and 310 K in the proton Larmor frequency range 0.01–70 MHz, corresponding to magnetic field strengths varying between 2.343×10^{-4} and 1.645 T. Let us consider first the relaxometric properties of the $[Gd_2(L^2)]$ complex (Figure 3). The relaxivity of $[Gd_2(L^2)]$ decreases with increasing temperature (Figure S11, Supporting Information), which shows that r_{1p} is limited by the fast rotation of the complex in solution, as usually observed for small, rapidly tumbling Gd^{III} chelates. When this occurs τ_M cannot be determined with accuracy from the analysis of the NMRD data. Thus, we have measured ^{17}O NMR chemical shifts and transverse relaxation rates and analyzed simultaneously the ^{17}O NMR and ^1H NMRD data using the Solomon–Bloembergen–Morgan theory[33] for the inner-sphere

relaxation mechanism and the Freed model[34] for the outer-sphere ^{1}H contribution to r_{1p}. However, the analysis of the ^{17}O NMR and NMRD data of [$Gd_2(L^2)$] is not straightforward due to the unique structure of this complex in solution. Indeed, the two metal coordination environments in this binuclear complex are not equivalent: one Gd^{III} ion being coordinated by the seven donor atoms of a DO3A unit and a nitrogen atom of the bipyridyl moiety (q=0, site I), while the second metal ion is bound to the second DO3A unit and two inner-sphere water molecules (q=1.8 as determined for the Eu^{III}complex, site II).[19] Thus, the Gd^{III} ion in site I is expected to provide only an outer-sphere contribution to r_{1p}, while that of site II should give rise to both inner- and outer-sphere contributions. Concerning the effect on ^{17}O NMR chemical shifts and relaxation rates, only the Gd^{III} ion in site II is expected to be responsible for the observed effects. Further evidence for the presence of two different coordination environments with q=0 and q approximately 2 is provided by the NMRD profiles recorded at pH 11.5 in the presence of an excess of Na_2CO_3. Under these conditions the observed r_{1p} is considerably lower than that measured at neutral pH, which is explained by the coordination of carbonate to the Gd^{III} ion in site II. Unfortunately, the NMRD profiles measured under these conditions cannot be used directly to estimate the outer-sphere contribution to r_{1p}, as the coordination of a highly charged anion such as CO_3^{2-} results in a substantial second-sphere contribution.

The analysis of the NMRD and ^{17}O NMR data of [$Gd_2(L^2)$] was performed under the assumption that the two Gd^{III} ions provide identical outer-sphere contributions to relaxivity. Satisfactory fits of the experimental NMRD curves were obtained by using the q value determined from luminescence lifetime measurements on the Eu^{III} analogue (q=1.8, Table 1). The distance between the proton nuclei of the coordinated water molecules and the Gd^{III}ion was fixed to 3.1 Å, while the distance of closest approach between the solute and solvent molecules was taken as 4.0 Å. Furthermore, the coefficient that describes the relative diffusion of solute and solvent molecules $\left(D_{\mathrm{GdH}}^{298}\right)$[35] was fixed to a common value. The relevant parameters obtained from the best-fit analysis of the data profiles are compared to those of [Gd(DO3A)], $[Gd(DOTA)]^-$ and [Gd_2{pip($DO3A)_2$}] in Table 2 (see Scheme 3 for the structures of the ligands). The last binuclear complex contains two DO3A units bridged by a 1,1′-(piperazine-1,4-diyl)diethanone moiety, and therefore possesses a size comparable to that of [$Gd_2(L^2)$].

Table 2. Parameters obtained from the analysis of the ^{17}O NMR and NMRD data for [$Gd_2(L^2)$].[a]

	[$Gd_2(L^2)$]	[Gd(DO3A)] [b]	[Gd(DOTA)] [c]	[Gd_2{pip($DO3A)_2$}] [c]
q	<u>1.8</u>	1.8	1	2
k_{ex}^{298} [10^6 s^{-1}]	(29.2±1.5)	11	4.1	1.5
$A/\hbar$ [10^6 rad s^{-1}]	(−3.9±0.8)	−3.9	−3.7	−3.8
τ_{R}^{298} [ps]	(185±2)	103	77	171
τ_{V}^{298} [ps]	(35.0±1.0)	27	11	19
Δ^2 [10^{20} s^{-2}]	(0.283±0.008)	0.30	0.16	0.17
D_{GdH}^{298} [10^{-10} m^2s^{-1}]	<u>25.0</u>	–	22	29
r_{GdH} [Å]	<u>3.1</u>	–	3.1	3.1
a_{GdH} [Å]	<u>4.0</u>	–	3.5	3.5

[a] Underlined values were fixed during the fitting procedures. [b] Data from ref. 40. [c] Data from ref. 36.

Our fits provide values for the electron relaxation parameters τ_{V}^{298} and Δ^2) quite similar to those obtained for the DO3A and DOTA analogues. Furthermore, the ^{17}O hyperfine coupling constant of the inner-sphere water molecules ($A/\hbar$) falls within the range generally observed for Gd^{III} complexes ($-3.6\times10^6\pm0.3$

rad s^{-1}),[37] which indicates that the hydration number determined from luminescence lifetime measurements is correct (q=1.8). The value of τ_R^{298} obtained for [$Gd_2(L^2)$] is longer than those determined for mononuclear Gd^{III} complexes, but close to those reported for different binuclear derivatives of similar molecular weight,[38,39] including [Gd_2{pip($DO3A)_2$}].[36] The outer-sphere contribution to relaxivity at 25 °C (Figure 3) represents about 40 % of the observed relaxivity in the proton Larmor frequency range 0.01–1.0 MHz, but this contribution drops to about 28 % at 60 MHz.

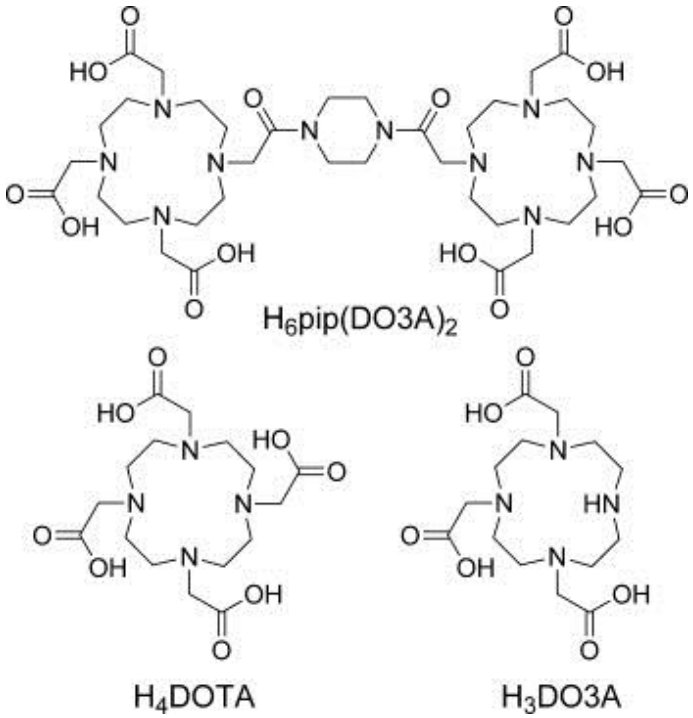

Scheme 3. Ligands used for comparative purposes in Table 2.

The water exchange of the inner-sphere water molecules determined for [$Gd_2(L^2)$] is about 2.5 times faster than in [Gd(DO3A)] and almost 7 times faster than for $[Gd(DOTA)]^-$. The water exchange of water molecules in nine-coordinate Gd^{III} complexes proceeds through a dissociatively activated mechanism, and its rate is closely related to the steric crowding around the water-binding site.[41] In the case of [$Gd_2(L^2)$] the presence of a bulky [Gd(DO3A)] unit with q=0 close to the nine-coordinated unit with q=2 might cause some steric hindrance around the coordinated water molecules. This would facilitate the departure of coordinated water molecules resulting in a fast exchange rate. The k_{ex} value determined for [$Gd_2(L^2)$] (29.2×10^6 s^{-1}, τ_M^{298}=34 ns) is close to the optimal values required to attain high relaxivities providing that τ_R is also optimized.[42]

The NMRD profiles recorded for [$Gd_2(L^1)$] and [$Gd_2(L^3)$] show a plateau at low field (0.01–3 MHz; Figure 4). In this region, relaxivity receives a significant contribution by the electron relaxation time. Above about 3 MHz the NMRD profiles of both compounds show a pronounced increase of r_{1p}, which reaches a maximum at about 20–30 MHz, and then decreases again at higher frequencies. Above about 3 MHz the inner contribution to r_{1p} is basically determined by the residence lifetime of the inner-sphere water molecule(s) (τ_M) and the rotational correlation time (τ_R). The peak observed in the region 8–60 MHz, which is clearly more pronounced in the case of [$Gd_2(L^3)$], is characteristic of slowly tumbling systems with τ_R values of the order of ns. Furthermore, the NMRD profiles of [$Gd_2(L^3)$] show reduced temperature dependence when compared to [$Gd_2(L^2)$], which indicates that both τ_R and $\tau_M$are limiting r_{1p} in [$Gd_2(L^1)$] and [$Gd_2(L^3)$]. Thus,

$[Gd_2(L^1)]$ and $[Gd_2(L^3)]$ show a nonconventional behavior that may be accounted for by self-aggregation of these complexes in aqueous solution. The longitudinal relaxation rate of aqueous solutions of $[Gd_2(L^3)]$ (R_1^{obs}) shows a linear dependence with Gd^{III}concentration (Figure S13 in the Supporting Information) in the range 0.1–1.8 mM, which indicates that the aggregates are stable in this concentration range, with no significant disaggregation occurring.

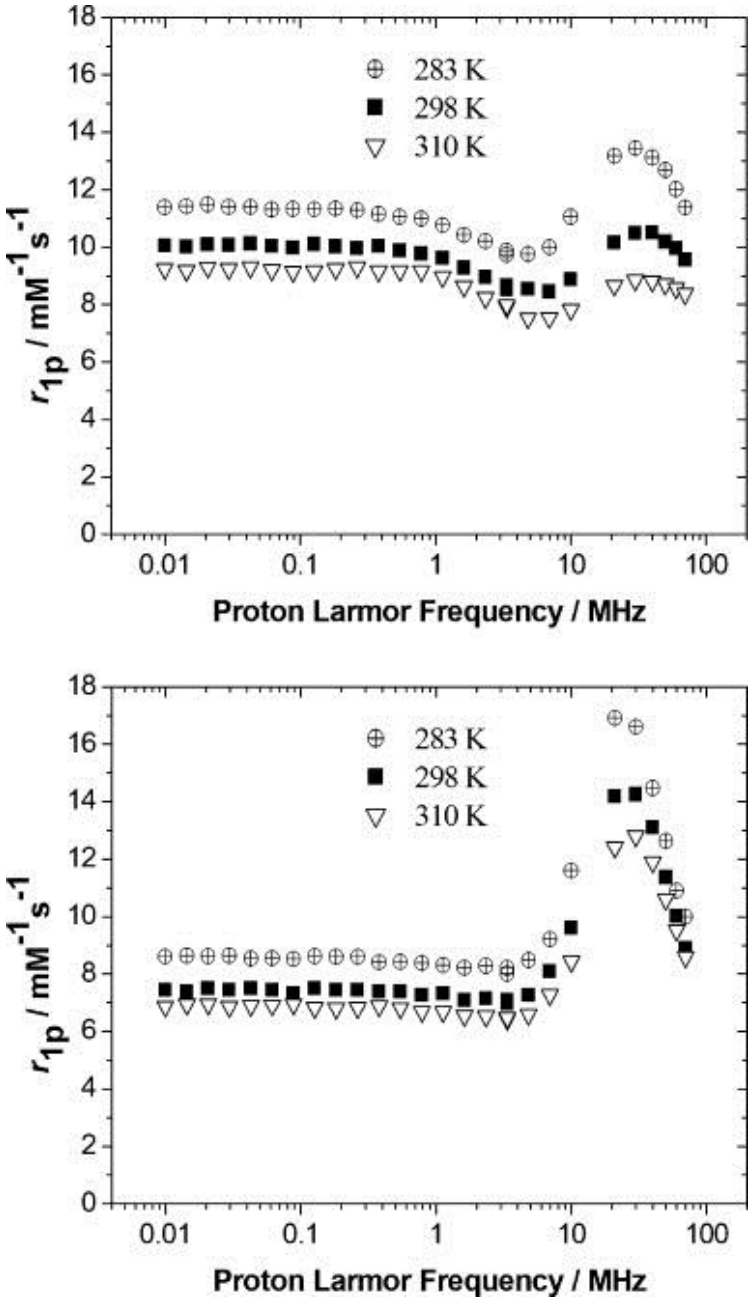

Figure 4. NMRD profiles recorded for $[Gd_2(L^1)]$ (4.8 mM; top) and $[Gd_2(L^3)]$ (1.7 mM; bottom) at different temperatures.

The NMRD profiles recorded for $[Gd_2(L^1)]$ and $[Gd_2(L^3)]$ were not analyzed to obtain rotational correlation times due to several reasons. First, the common Solomon–Bloembergen–Morgan theory cannot be used to fit NMRD profiles of slowly rotating molecules at low fields. Second, theoretical predictions show that large particles (see below) with rotational correlation times of 10 ns and longer should give much higher

relaxivities (well above 40 $mM^{-1} s^{-1}$).[43] A possible explanation for a lower relaxivity could be an important degree of flexibility of the aggregates, but this is unlikely in the case of large three-dimensional particles. Thus, the relatively low relaxivities measured for [$Gd_2(L^1)$] and [$Gd_2(L^3)$] are most likely related to the nonporous nature of the aggregates, which probably prevents the access of water molecules in proximity of the paramagnetic ions located in the interior of the particles. As a consequence, only Gd^{III} ions at the surface of the particles contribute to relaxivity. This situation is common for Gd-based inorganic nanoparticles and it has been recently analyzed in some detail.[44]

Characterization of the aggregates

The nature of the aggregates, whose presence is suggested by the shape and amplitude of the NMRD profiles, was investigated by using different experimental techniques. In a first set of experiments, we recorded ESI-TOF mass spectra of solutions of [$Gd_2(L^3)$] in ammonium acetate buffer (0.013 M, pH 6.7). The MS clearly show a peak at *m*/*z* 1226.25 corresponding to the $[Gd_2L^3+CH_3COO]^-$ entity, which is superimposed to a peak attributed to the corresponding dimer $[2\,Gd_2L^3+2\,CH_3COO]^{2-}$(Figure S14 in the Supporting Information). Very weak peaks (less than 3 % of the maximum intensity) could also be observed at *m*/*z* 1913 and 2532, which may be attributed to $[3\,Gd_2L^3+2\,CH_3COO]^{2-}$ and $[2\,Gd_2L^3+CH_3COO]^-$, suggesting the formation of aggregates in solution even at high dilutions ($<10^{-4}$ M).

Dynamic light scattering (DLS) experiments were carried out at 298 K on aqueous solutions (pH 7.2) of [$Gd_2(L^1)$] and [$Gd_2(L^3)$] filtered through 450 nm filters. Peaks were found with a maximum corresponding to 114 (0.30) and 38 nm (0.15 polydispersity index) for [$Gd_2(L^1)$] and [$Gd_2(L^3)$], respectively (Figure 5). This supports the hypothesis that these complexes tend to form relatively large aggregates in solution. In agreement with the corresponding relaxometric data, no variations were observed upon dilution of the solutions over the range 0.1–1.2 mM.

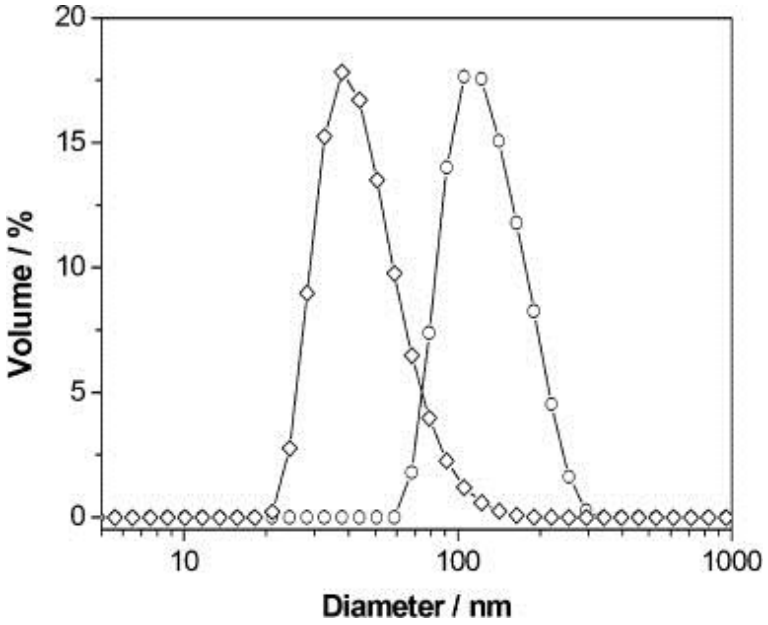

Figure 5. DLS data for [$Gd_2(L^1)$] (circles; 114 nm and 0.15 PDI) and for [$Gd_2(L^3)$] (diamonds; 38 nm and 0.30 PDI) in aqueous solution at neutral pH (1.2 mM). The solid lines are simply a guide for the eye.

Information on the shape and size of the particles formed by [$Gd_2(L^3)$] was obtained from transmission electron microscopy (TEM) experiments (Figure 6). Most of the particles appeared to be spherical with a

mean diameter of 41 nm, in good agreement with the DLS data. Additionally, some larger nonspherical particles are also observed (Figure 6). The particles have a large electron density, which reflects a high Gd content.

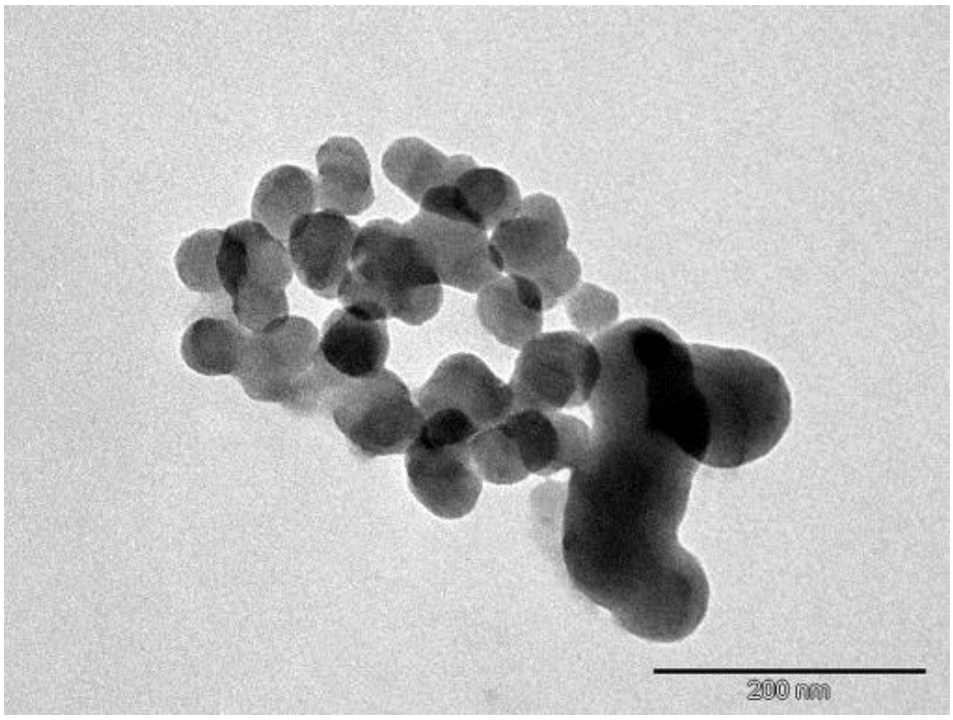

Figure 6. A typical TEM image obtained for $[Gd_2(L^3)]$. Spherical particles with an average diameter of 41 nm are observed together with fewer nonspherical particles with larger size.

Aggregation of binuclear Gd^{III} complexes was observed previously by using ligands that contain two DO3A units linked by a xylene core as a non-coordinating unit.[45] The authors suggested that self-aggregation could be related to hydrophobic interactions, π stacking between the aromatic linker, or hydrogen bonding between the chelates. A mononuclear Gd^{III} complex with a podand bearing four 3-carboxylate pyrazole arms and a phenyl core was also shown to aggregate into spherical porous nanoparticles.[46] In this last case the authors suggested that the formation of self-aggregates originated from weak intermolecular interactions and not from strong metal–ligand bonds inducing polymerization. We believe that in the case of $[Gd_2(L^1)]$ and $[Gd_2(L^3)]$ aggregation is related to the presence of bridging carboxylate units that connect neighboring binuclear entities, probably assisted by intermolecular π stacking interactions involving the aromatic linker. There is a certain amount of evidence to support this hypothesis:

1) Different examples of lanthanide complexes forming oligomeric or polymeric units in the solid state, due to the presence of bridging bidentate carboxylate groups, have been reported in the literature.[47,48]

2) No evidence for aggregation was observed for binuclear lanthanide complexes based on two DOTA units separated by aromatic linkers. The octadentate nature of the chelating units leaves place for the coordination of a water molecule, but prevents the formation of carboxylate bridges between the two metal centers.[26a,49]

3) Luminescence lifetime measurements provided *q* values of 1, within experimental error, for the $[Ln_2(L^1)]$ complexes (Ln=Eu or Tb, Table 1). Being DO3A derivatives, one would expect a

hydration number closer to 2, and therefore a low hydration number is compatible with the presence of bridging carboxylate groups. The 4,4′-dimethyl-2,2′-bipyridyl linker of $[Ln_2(L^1)]$ cannot coordinate to the Ln^{III} ion, and therefore aggregation via the formation of carboxylate bridging units is possible. In contrast, the 6,6′-dimethyl-2,2′-bipyridyl linker of $[Ln_2(L^2)]$ complexes coordinates to the metal ion, thereby preventing aggregation.

To make a rough estimation of the number of $[Ln_2(L^3)]$ units contained in a typical aggregate, we performed theoretical calculations on the $[Gd_2(L^3)(H_2O)_2]$ system at the HF and B3LYP levels (see Computational Methods section). The minimum energy conformation obtained for $[Gd_2(L^3)(H_2O)_2]$ shows a square-antiprismatic coordination environment around the metal ions, which are each coordinated to the four nitrogen atoms of the macrocycle, three oxygen atoms of carboxylate groups, an oxygen atom of a water molecule, and a nitrogen atom of a pyrazolyl unit. Most likely, the pyrazolyl nitrogen atom is replaced by an oxygen atom of a carboxylate group belonging to a neighboring molecule upon aggregation. The molecular volume of $[Gd_2(L^3)(H_2O)_2]$, defined as the volume inside a contour density of 0.001 e $Bohr^{-3}$, amounts to 1078 $Å^3$. Thus, considering the volume of a typical spherical particle of 38 nm, we estimate that each particle may contain up to about 2.7×10^4 $[Gd_2(L^3)(H_2O)_2]$ units.

An important requirement of any potential bimodal probe for application in MRI and optical imaging is a high stability under physiological conditions. In the case of $[Gd_2(L^1)]$ and $[Gd_2(L^3)]$, the DO3A coordinating units are expected to provide enough thermodynamic and kinetic stability to the corresponding complexes. Additionally, the stability of the formed aggregates in biological media is also important. Thus, the stability with time of a 1.17 mMsolution of $[Gd_2(L^3)]$ in a lyophilized serum of human origin (Seronorm) was assessed by relaxometric measurement at 0.5 T and 310 K. The complex proved to be stable at least over 96 h (Figure 7). Only very small and negligible fluctuations in the relaxation rate data were detected, well within the experimental error (±3–4 %). A similar situation is observed for $[Gd_2(L^2)]$, which was proved to be stable at least over 52 h (Figure S15 in the Supporting Information). These results thus indicate that the DO3A derivatives reported here do not experience dissociation in serum, nor particle disaggregation.

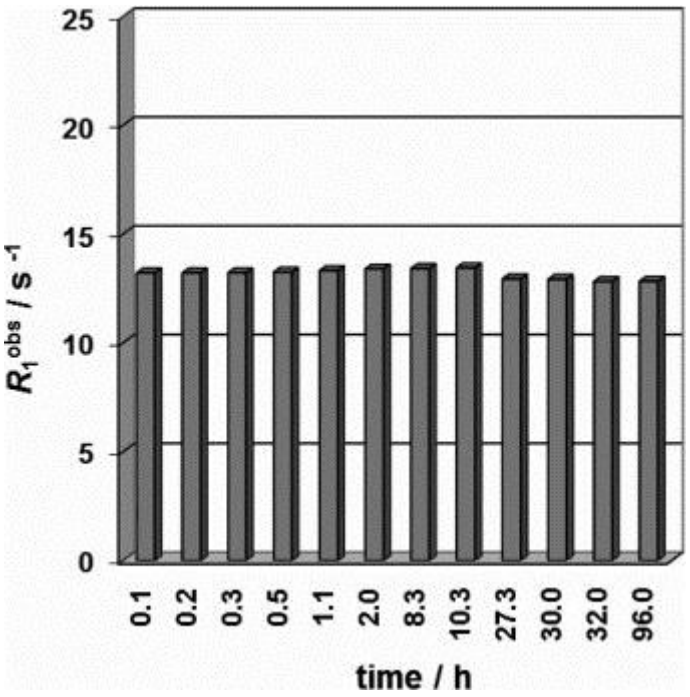

Figure 7. Proton relaxation rate at 0.5 T and 310 K of a 1.17 mM solution of $[Gd_2(L^3)]$ in Seronorm as a function of time.

Conclusion

Binuclear Ln^{III} complexes with bis-macrocyclic ligands L^1 and L^3, which contain two DO3A units linked by 4,4′-dimethyl-2,2′-bipyridine and 2,6-bis(1*H*-pyrazol-1-yl)pyridine spacers, respectively, form nanosized aggregates stable in aqueous solutions and serum. In contrast, the complexes of L^2, which contain a 6,6′-dimethyl-2,2′-bipyridyl spacer, do not aggregate probably due to the coordination of the bipyridyl moiety to one of the Ln^{III} ions. As a result, the $[Gd_2(L^1)]$ and $[Gd_2(L^3)]$ complexes have high relaxivities, the NMRD profiles showing a characteristic pronounced increase of r_{1p} above 3 MHz that reaches a maximum at about 20–30 MHz. The $[Gd_2(L^2)]$ complex, however, provides NMRD profiles characteristic of rapidly tumbling complexes, relaxivity being limited by the fast rotation of the complex in solution. Interestingly, the simultaneous analysis of the NMRD and ^{17}O NMR data of $[Gd_2(L^2)]$ indicates a relatively fast water exchange of the inner-sphere water molecules (k_{ex}^{298}=29.2×10^6 s^{-1}).

Besides quite high relaxivities, the $[Ln_2(L^1)]$ and $[Ln_2(L^3)]$ (Ln=Eu or Tb) complexes also present high quantum yields of the Ln^{III}-centered emission upon excitation through the ligand levels. In the case of $[Tb_2(L^3)]$, the quantum yield of the Tb^{III}-centered emission is particularly high (50 %). Considering that the relaxivity of $[Gd_2(L^3)]$ is also substantially higher than that of $[Gd_2(L^1)]$, L^3 appears to be a good candidate for the preparation of bimodal probes for MRI and optical imaging. Furthermore, taking together the results reported in this paper and the work of Merbach et al.,[45] it appears that there is a general trend of coordinatively unsaturated Ln^{III} complexes with ligands containing two DO3A units linked by aromatic non-coordinating units to form stable aggregates in aqueous solutions. This discovery may be used for the design of new Ln^{III}-based nanosized materials for application in different imaging modalities.

Experimental section

General methods

Elemental analyses were carried out on a Carlo Erba 1108 elemental analyzer. High-resolution ESI-TOF mass spectra were recorded using a LC-Q-q-TOF Applied Biosystems QSTAR Elite spectrometer in the positive mode (Concentration ca. 10^{-4} M, Solvent: MeOH/CH_3CN/H_2O 9:1:1), or a microQTOF-Q Bruker Daltonics spectrometer in the negative mode. IR-spectra were recorded using a Bruker Vector 22 spectrophotometer equipped with a golden gate attenuated total reflectance (ATR) accessory (Specac). ^1H and ^{13}C NMR spectra were recorded at 25 °C on Bruker Avance 300 and Bruker Avance 500 MHz spectrometers. For measurements in D_2O, *tert*-butyl alcohol was used as an internal standard with the methyl signal calibrated at δ=1.2 (^1H) and 31.2 ppm (^{13}C).

Absorption and emission electronic spectra

UV/Vis absorption spectra were recorded on a Specord 205 (Analytik Jena) spectrometer. Steady state emission and excitation spectra were recorded on a Horiba Jobin Yvon Fluorolog 3 spectrometer working with a continuous 450 W Xe lamp. Detection was performed with a Hamamatsu R928 photomultiplier. All spectra were corrected for the instrumental functions. When necessary, a 399 nm cutoff filter was used to eliminate the second order artifacts. Phosphorescence lifetimes were measured on the same instrument working in the phosphorescence mode, with 50 μs delay time and a 100 ms integration window and fitted with the FAST program from Edinburgh Instrument. Hydrations numbers (q) were obtained using Equation (1),[28] in which τ_{H_2O} and τ_{D_2O} refer to the measured luminescence decay lifetimes (in ms) in water and deuterated water, respectively, using A_{Eu}=1.2 and a_{Eu}=0.25 for Eu^{III} and A_{Tb}=5.0 and a_{Tb}=0.06 for Tb^{III}:

$$q = A_{\mathrm{Ln}}\left(1/\tau_{\mathrm{H_2O}} - 1/\tau_{\mathrm{D_2O}} - a_{\mathrm{Ln}}\right) \quad (1)$$

Luminescence quantum yields were measured according to conventional procedures,[50] with diluted solutions (optical density <0.05), using $[Ru(bpy)_3]Cl_2$ in nondegassed water (Φ=4.0 %),[29] rhodamine 6G in water (Φ=76.0 %)[30] as references. Estimated errors are ±15 %.

Water proton relaxivity measurements

The water proton longitudinal relaxation rates as a function of temperature (20 MHz) were measured with a Stelar Spinmaster Spectrometer (Mede, Pv, Italy) on about 0.8–2.0 mM aqueous solutions in nondeuterated water. The exact concentrations of gadolinium were determined by measurement of bulk magnetic suceptibility shifts of a *t*BuOH signal on a Bruker Avance III 500 spectrometer (11.7 T).[51] The ^{1}H T_1 relaxation times were acquired by the standard inversion recovery method with typical 90° pulse width of 3.5 μs, 16 experiments of 4 scans. The reproducibility of the T_1 data was ±5 %. The temperature was controlled with a Stelar VTC-91 airflow heater equipped with a calibrated copper-constantan thermocouple (uncertainty of ±0.1 °C). The proton $1/T_1$ NMRD profiles were measured on a fast field-cycling Stelar SmartTracer relaxometer over a continuum of magnetic field strengths from 0.00024 to 0.25 T (corresponding to 0.01–10 MHz proton Larmor frequencies). The relaxometer operates under computer control with an absolute uncertainty in $1/T_1$ of ±1 %. Additional data points in the range 15–70 MHz were obtained using a Stelar Relaxometer Consolle connected to a Bruker WP80 NMR electromagnet adapted to variable-field measurements.

^{17}O NMR measurements

Variable-temperature ^{17}O-NMR measurements were recorded on the Bruker Avance III 500 spectrometer (11.7 T), equipped with a 5 mm probe. Experimental settings: spectral width 13 000 Hz, 90° pulse (18 μs), acquisition time 600 ms, 256 scans, and no sample spinning. Aqueous solutions of the complex (ca. 20 mM) containing 2.0 % of the ^{17}O isotope (Cambridge Isotope) were used. The observed transverse relaxation rates (R_2) were calculated from the signal width at half-height. The bulk magnetic susceptibility contribution was subtracted from the ^{17}O NMR shift data using the ^{1}H NMR shifts of the *t*BuOH signal as internal reference.

Dynamic light scattering (DLS)

The assessment of size and size distribution for the aggregated complexes were analyzed by Malvern Zeta Sizer Nanoinstrument (NanoZS, Malvern, UK). The Zetasizer software extracts the decay rate of the autocorrelation function by means of the routinely cumulant analysis. At the end of the analysis, the instrument gives the results in terms of sizes distribution as defined by the Stokes–Einstein equation. The wavelength of the laser light (He/Ne) was 633 nm. The mean aggregate size diameter (*z*-average) and the polydispersity index (PDI) were issued from scattered light intensity results. Each measurement was performed in triplicate at 298 K and both the aggregate *z*-average diameter and PDI were determined.

Transmission electron microscopy (TEM)

The sizes of the nanosized aggregates were examined by transmission electron microscopy (TEM). The samples were prepared by placing drops of the a solution containing the aggregates on a Formvar coated copper grid (Electron Microscopy Sciences, 200 mesh), followed by drying in air. The TEM images were obtained with a Jeol JEM 1100 instrument operating at a 80 kV accelerating voltage.

Chemicals and starting materials

2,6-Bis(3-bromomethyl-1-pyrazolyl)pyridine (**1**)[23] and $[Gd_2(L^2)]\cdot 4\,H_2O$[19] were prepared according to literature methods. All other chemicals were purchased from commercial sources and used without further purification, unless otherwise stated. Neutral Al_2O_3 (Fluka, 0.05–0.15 mm) was used for preparative column chromatography.

2,6-Bis{3-[4,7,10-tris(*tert*-butoxycarbonylmethyl)-1,4,7,10-tetraazacyclododecane-1-ylmethyl]-1*H*-pyrazol-1-yl}pyridine (2)

A mixture of DO3A(*t*BuO)$_3$ (0.500 g, 0.971 mmol) and Na_2CO_3 (0.237 g, 2.23 mmol) in acetonitrile (25 mL) was stirred for 30 min and then 2,6-bis(3-bromomethyl-1-pyrazolyl)pyridine (0.193 g, 0.486 mmol) and a catalytic amount of KI were added. The mixture was heated to reflux with stirring under an inert atmosphere (Ar) for a period of 24 h, and then the excess of Na_2CO_3 was filtered off. The filtrate was concentrated to dryness and the yellow oil was extracted with a mixture of H_2O and CH_2Cl_2(1:3; 100 mL). The organic phase was evaporated to dryness to give an oily residue that was purified by column chromatography on Al_2O_3 with a CH_2Cl_2/MeOH 5 % mixture as the eluent to give 0.544 g of **2** as a yellow foam. Yield 78 %; elemental analysis calcd (%) for $C_{65}H_{109}N_{13}O_{12}\cdot 2\,CH_2Cl_2$: C 56.10, H 7.94, N 12.69; found: C 55.92, H 7.72, N, 12.47; MS (ESI$^+$, MeOH/CH_3CN/H_2O 9:1:1): *m*/*z*: 633 $[C_{65}H_{111}N_{13}O_{12}]^{2+}$; IR (ATR): $\tilde{\nu}$=1724 (C=O), 1606, 1589 cm^{-1} (C=N and C=C); ^{1}H NMR ($CDCl_3$, 500 MHz, 25 °C, TMS): δ=8.44 (d, ^3J=2.6 Hz, 2 H; PzH), 7.91 (d, ^3J=8.1 Hz, 2 H; PyH), 7.72 (t, ^3J=8.1 Hz, 1 H; PyH), 6.61 (d, ^3J=2.6 Hz, 2 H; PzH), 3.66–1.75 (m, 48 H; -NCH_2), 1.49–1.46 ppm (m, 54 H; *t*BuO-); ^{13}C NMR ($CDCl_3$, 125.8 MHz, 25 °C, TMS): δ=172.9, 172.6 (CO), 153.0 (Pz), 149.7, 141.1 (Py), 127.9 (Pz), 109.9 (Py), 109.0 (Pz), 82.1, 82.0, 56.3, 55.9, 51.4, 50.1, 31.8 (-NCH_2), 28.0, 27.8 ppm (*t*BuO-).

2,6-Bis{3-[4,7,10-tris(carboxymethyl)-1,4,7,10-tetraazacyclododecane-1-ylmethyl]-1*H*-pyrazol-1-yl}pyridine hexatrifluoroacetate (H_6L^3)

Compound **2** (0.544 g, 0.379 mmol) was dissolved in a 1:1 mixture of water and trifluoroacetic acid (10 mL). The mixture was heated to reflux with stirring for 24 h and then the solvents were removed in a rotary evaporator to give a brown oil. This was dissolved in MeOH (10 mL) and the solvent evaporated. This process was repeated twice, and then three times with CH_2Cl_2. The oily residue was dissolved in MeOH (1 mL) and diethyl ether was added until the precipitation of a white solid was complete. The white solid was isolated by filtration and dried under vacuum to give 0.522 g of the desired compound. Yield 81 %; elemental analysis calcd (%) for $C_{41}H_{61}N_{13}O_{12}\cdot 6\,CF_3COOH\cdot 5\,H_2O$: C 37.40, H 4.56, N 10.70; found: C 37.62, H 4.47, N 10.56; MS (ESI$^+$, MeOH/CH_3CN/H_2O 9:1:1): *m*/*z*: 928 $[C_{41}H_{62}N_{13}O_{12}]^+$, 465 $[C_{41}H_{63}N_{13}O_{12}]^{2+}$; IR (ATR): $\tilde{\nu}$=3416 (O-H), 1673, 1607, 1588 cm^{-1} (C=O); ^{1}H NMR (D_2O, pD 2.0, 500 MHz, 25 °C, TMS): δ=8.51 (s, 2 H; PzH), 8.02 (t, ^3J=7.9 Hz, 1 H; PyH), 7.63 (d, ^3J=7.9 Hz, 2 H; PyH), 6.74 (s, 2 H; PzH), 4.13–3.02 ppm (m, 48 H; -NCH_2); ^{13}C NMR (D_2O, pD 2.0, 125.8 MHz, 25 °C, TMS): δ=174.7, 171.8 (CO), 150.6, 144.3 (Py), 132.3, 112.3 (Pz), 111.9 (Py), 111.3 (Pz), 56.1, 55.6, 52.5, 51.8, 51.6, 50.7, 50.0 ppm (-NCH_2).

General procedure for the preparation of $[Ln_2(L^3)]\cdot 2\,H_2O$ complexes

A mixture of $H_6L^3\cdot 6\,CF_3COOH\cdot 5\,H_2O$ (0.100 g, 0.059 mmol), triethylamine (0.071 g, 0.705 mmol), and Ln(OTf)$_3$(0.117 mmol, Ln=La, Eu, Gd, Tb, Yb or Lu) in 2-propanol (10 mL) was heated to reflux for 24 h. The reaction was allowed to cool to room temperature, resulting in the formation of a white precipitate that was washed with MeOH and diethyl ether. The mother liquor was stored at 4 °C for several days, resulting in the formation of a second batch of complex that was again collected by filtration and washed with MeOH and diethyl ether.

$[La_2(L^3)]\cdot 2\,H_2O$: Yield 0.064 g, 88 %; elemental analysis calcd (%) for $C_{41}H_{55}La_2N_{13}O_{12}\cdot 2\,H_2O$: C 39.85, H 4.81, N 14.73; found: C 39.66, H 4.59, N 14.58; HR-MS (ESI^+, MeOH/CH_3CN/H_2O 9:1:1): *m*/*z* calcd for $[C_{41}H_{57}La_2N_{13}O_{12}]^{2+}$: 600.6182; found: 600.6157; IR (ATR): $\tilde{\nu}$=1575 cm^{-1}(C=O).

$[Eu_2(L^3)]\cdot 2\,H_2O$: Yield 0.067 g, 90 %; elemental analysis calcd (%) for $C_{41}H_{55}Eu_2N_{13}O_{12}\cdot 2\,H_2O$: C 39.02, H 4.71, N 14.43; found: C 38.86, H 4.56, N 14.28; HR-MS (ESI^+, MeOH/CH_3CN/H_2O 9:1:1): *m*/*z* calcd for $[C_{41}H_{57}Eu_2N_{13}O_{12}]^{2+}$: 614.6331; found: 614.6354; *m*/*z* calcd for $[C_{41}H_{56}Eu_2N_{13}O_{12}]^+$ 1228.2590; found: 1228.2586; IR (ATR): $\tilde{\nu}$=1583 cm^{-1} (C=O).

$[Gd_2(L^3)]\cdot 2\,H_2O$: Yield 0.068 g, 91 %; elemental analysis calcd (%) for $C_{41}H_{55}Gd_2N_{13}O_{12}\cdot 2\,H_2O$: C 38.70, H 4.67, N 14.31; found: C 38.87, H 4.91, N 14.38; HR-MS (ESI^+, MeOH/CH_3CN/H_2O 9:1:1): *m*/*z* calcd for $[C_{41}H_{57}Gd_2N_{13}O_{12}]^{2+}$: 619.6360; found: 619.6380; *m*/*z* calcd for $[C_{41}H_{55}Gd_2N_{13}NaO_{12}]^+$: 1260.2467; found: 1260.2487; IR (ATR): $\tilde{\nu}$=1583 cm^{-1} (C=O).

$[Tb_2(L^3)]\cdot 2\,H_2O$: Yield 0.067 g, 89 %; elemental analysis calcd (%) for $C_{41}H_{55}N_{13}O_{12}Tb_2\cdot 2\,H_2O$: C 38.60, H 4.66, N 14.27; found: C 38.49, H 4.83, N 14.32; HR-MS (ESI^+, MeOH/CH_3CN/H_2O 9:1:1): *m*/*z* calcd for $[C_{41}H_{57}N_{13}O_{12}Tb_2]^{2+}$: 620.6372; found: 620.6400; *m*/*z* calcd for $[C_{41}H_{56}N_{13}O_{12}Tb_2]^+$: 1240.2672; found: 1240.2634; IR (ATR): $\tilde{\nu}$=1584 cm^{-1} (C=O).

$[Yb_2(L^3)]\cdot 2\,H_2O$: Yield 0.067 g, 87 %; elemental analysis calcd (%) for $C_{41}H_{55}N_{13}O_{12}Yb_2\cdot 2\,H_2O$: C 37.76, H 4.56, N 13.96; found: C 38.02, H 4.73, N 13.72, HR-MS (ESI^+, MeOH/CH_3CN/H_2O 9:1:1): *m*/*z* calcd for $[C_{41}H_{55}N_{13}Na_2O_{12}Yb_2]^{2+}$: 657.6327; found: 657.6343; *m*/*z* calcd for $[C_{41}H_{55}N_{13}NaO_{12}Yb_2]^+$: 1292.2762; found: 1292.2719; IR (ATR): $\tilde{\nu}$=1585 cm^{-1} (C=O).

$[Lu_2(L^3)]\cdot 2\,H_2O$: Yield 0.068 g, 88 %. elemental analysis calcd (%) for $C_{41}H_{55}Lu_2N_{13}O_{12}\cdot 2\,H_2O$: C 37.65, H 4.55, N 13.92; found: C 37.52, H 4.76, N 13.75; HS-MS (ESI^+, MeOH/CH_3CN/H_2O 9:1:1): *m*/*z* calcd for $[C_{41}H_{57}Lu_2N_{13}O_{12}]^{2+}$: 636.6527; found: 636.6547; *m*/*z* calcd for $[C_{41}H_{56}Lu_2N_{13}O_{12}]^+$: 1272.2981; found: 1272.2937; IR (ATR): $\tilde{\nu}$=1587 cm^{-1} (C=O); ^{1}H NMR (D_2O, pD 7.0, 500 MHz, 25 °C, TMS): δ=8.53 (m, 2 H), 8.13 (m, 1 H), 7.61 (m, 2 H), 6.64 (m, 2 H), 4.31–2.60 ppm (m, 48 H); ^{13}C NMR (D_2O, pD 7.0, 125.8 MHz, 25 °C, TMS): δ=182.7, 182.1, 181.1, 156.1, 150.7, 144.5, 136.6, 116.1, 110.4, 67.8, 67.0, 61.7, 60.8, 57.7, 57.0, 56.7, 55.8, 54.8, 53.5, 51.8, 50.0 ppm.

$[Gd_2(L^1)]\cdot 6\,H_2O$: A mixture of $H_6L^1\cdot 6\,CF_3COOH\cdot 3\,H_2O$[20] (0.100 g, 0.062 mmol), triethylamine (0.075 g, 0.744 mmol), and $Gd(OTf)_3$ (0.075 g, 0.124 mmol) in 2-propanol (10 mL) was heated to reflux for 24 h. The reaction was allowed to cool to room temperature, resulting in the formation of a white precipitate that was washed with MeOH and diethyl ether. The mother liquor was stored at 4 °C for several days, resulting in the formation of a second batch of complex that was again collected by filtration and washed with MeOH and diethyl ether. Yield 0.062 g, 77 %; elemental analysis calcd (%) for $C_{40}H_{54}Gd_2N_{10}O_{12}\cdot 6\,H_2O$: C 37.26, H 5.16, N 10.86; found: C 37.01, H 4.91, N 10.78; HS-MS (ESI^+, MeOH/CH_3CN/H_2O 9:1:1): *m*/*z* calcd for $[C_{40}H_{56}Gd_2N_{10}O_{12}]^{2+}$: 592.1275; found: 592.1298; IR (ATR): $\tilde{\nu}$=1581 cm^{-1} (C=O).

Computational methods

All calculations were performed employing the Gaussian 09 package (Revision A.02).[52] Full geometry optimizations of the $[Gd_2(L^3)(H_2O)_2]$ systems were performed at the HF level by using the effective core potential (ECP) of Dolg et al.,[53] the related [5s4p3d]-GTO valence basis set for the lanthanides,[53] and the 3-21G basis set for C, H, N, and O atoms. Although small, HF calculations employing this basis set in combination with the *f*-in-core ECP of Dolg were shown to provide molecular geometries of Ln^{III}–dota-like complexes in good agreement with the experimental structures observed by single-crystal X-ray diffraction studies.[54] No symmetry constraints were imposed during the optimizations. The stationary points found on the potential energy surfaces as a result of the geometry optimizations were tested to represent energy

minima rather than saddle points by means of a frequency analysis. The relative free energies of the different conformations obtained from geometry optimizations were calculated at the same computational level, and they include nonpotential-energy contributions (zero point energies and thermal terms) obtained through frequency analysis. Selected geometries optimized at the HF level were subsequently fully optimized by using hybrid DFT with the B3LYP exchange-correlation functional,[55] and the standard 6-31G(d) basis set for the ligand atoms. Due to the considerable computational effort involving the calculation of second derivatives at this level the optimized geometries were not characterized by using frequency analysis. Molecular volumes, defined as the volume inside a contour of 0.001 e $Bohr^{-3}$, were calculated at the B3LYP/6-31G(d) level by using the volume=tight keyword in Gaussian 09.

Acknowledgements

M. R.-F., D. E.-G., A. de B., T. R.-B. and C. P.-I. thank Ministerio de Educación y Ciencia (MEC, CTQ2009-10721), Fondo Europeo de Desarrollo Regional (FEDER, CTQ2009-10721) and Xunta de Galicia (IN845B-2010/063) for financial support. This research was performed in the frameworks of the EU COST Actions D38 “Metal-Based Systems for Molecular Imaging Applications” and CM1006 “EUFEN: European F-Element Network”. The authors are indebted to Centro de Supercomputación de Galicia (CESGA) for providing the computer facilities. A.N. and L.J.C. gratefully acknowledge the financial support of the French Centre National de la Recherche Scientifique, the University of Strasbourg and the European Commission (NANOGNOSTICS, n°242264). M.B. and G.R. are grateful to MIUR (PRIN 2009) for financial support. M.R.-F. also thanks the Ministerio de Educación y Ciencia (FPU program) for a predoctoral fellowship.

References

[1] a) C. M. G. dos Santos, A. J. Harte, S. J. Quinn, T. Gunnlaugsson, *Coord. Chem. Rev.* **2008**, *252*, 2512–2527; b) L. S. Natrajan, *Current Inorg. Chem.* **2011**, *1*, 61–75; c) E. Brunet, O. Huanes, J. C. Rodriguez-Ubis, *Current Chem. Biol.* **2007**, *1*, 11–39; d) L. J. Charbonnière, *Current Inorg. Chem.* **2011**, *1*, 2–16; e) J. Xu, T. M. Corneillie, E. G. Moore, G.-L. Law, N. G. Butlin, K. N. Raymond, *J. Am. Chem. Soc.***2011**, *133*, 19900–19910.

[2] *The Chemistry of Contrast Agents in Medical Magnetic Resonance Imaging* (Eds.: A. E. Merbach, L. Helm E. Toth), 2nd ed., Wiley, New York, **2013**.

[3] a) P. Caravan, J. J. Ellinson, T. J. McMurry, R. B. Lauffer, *Chem. Rev.* **1999**, *99*, 2293–2352; b) K. W.-Y. Chan, W.-T. Wong, *Coord. Chem. Rev.* **2007**, *251*, 2428–2451; c) E. Terreno, D. Delli Castelli, A. Viale, S. Aime, *Chem. Rev.* **2010**, *110*, 3019–3042; d) A. Datta, K. N. Raymond, *Acc. Chem. Res.* **2009**, *42*, 938–947.

[4] S. Cheng, L. Abramova, G. Saab, G. Turabelidze, P. Patel, M. Arduino, T. Hess, A. Kallen, M. Jhung, *JAMA J. Am. Med. Assoc.* **2007**, *297*, 1542–1544.

[5] "Stability and Toxicity of Contrast Agents": E. Brücher, A. D. Sherry, in *The Chemistry of Contrast Agents in Medical Magnetic Resonante Imaging* (Eds.: A. E. Merbach, É. Tóth), Wiley, Chichester, **2001**, pp. 243–279.

[6] a) B. Alpha, J.-M. Lehn, G. Mathis, *Angew. Chem.* **1987**, *99*, 259–261; *Angew. Chem. Int. Ed. Engl.* **1987**, *26*, 266–267; b) B. Alpha, R. Ballardi, V. Balzani, J.-M. Lehn, S. Perathoner, N. Sabbatini, *Photochem. Photobiol.***1990**, *52*, 299–306.

[7] R. Uppal, K. L. Ciesienski, D. B. Chonde, G. S. Loving, P. Caravan, *J. Am. Chem. Soc.* **2012**, *134*, 10799–10802.

[8] M. Sun, D. Hoffman, G. Sundaresan, L. Yang, N. Lamichhane, J. Zweit, *Am. J. Nucl. Med. Mol. Imaging* **2012**, *2*, 122–135.

[9] a) A. Keliris, T. Ziegler, R. Mishra, R. Pohmann, M. G. Sauer, K. Ugurbil, J. Engelmann, *Bioorg. Med. Chem.* **2011**, *19*, 2529–2540; b) A. B. Bourlinos, A. Bakandritsos, A. Kouloumpis, D. Gournis, M. Krysmann, E. P. Giannelis, K. Polakova, K. Safarova, K. Hola, R. Zboril, *J. Mater. Chem.* **2012**, *22*, 23327–23330; c) H. Yang, L. Ding, L. An, Z. Xiang, M. Chen, J. Zhou, F. Li, D. Wu, S. Yang, *Biomaterials* **2012**, *33*, 8591–8599; d) D. Dong, X. Jing, X. Zhang, X. Hu, Y. Wu, C. Duan, *Tetrahedron* **2012**, *68*, 306–310; e) S. Claudel-Gillet, J. Steibel, N. Weibel, T. Chauvin, M. Port, I. Raynal, E. Toth, R. Ziessel, L. J. Charbonnière, *Eur. J. Inorg. Chem.* **2008**, 2856–2862; f) A. Nonat, C. Gateau, P. H. Fries, L. Helm, M. Mazzanti, *Eur. J. Inorg. Chem.* **2012**, 2049–2061.

[10] M. Latva, H. Takalo, V.-M. Mukkala, C. Matachescu, J. C. Rodriguez-Ubis, J. Kankare, *J. Lumin* **1997**, *75*, 149–169.

[11] W. D. Horrocks, Jr., D. R. Sudnick, *J. Am. Chem. Soc.* **1979**, *101*, 334–340.

[12] E. Pérez-Mayoral, V. Negri, J. Soler-Padros, S. Cerdan, P. Ballesteros, *Eur. J. Radiol.* **2008**, *67*, 453–458.

[13] G. Angelovski, I. Mamedov, *Current Inorg. Chem.* **2011**, *1*, 76–90.

[14] a) E. J. Werner, A. Datta, C. J. Jocher, K. N. Raymond, *Angew. Chem.* **2008**, *120*, 8696–8709; *Angew. Chem. Int. Ed.* **2008**, *47*, 8568–8580; b) S. Aime, M. Botta, E. Terreno, *Adv. Inorg. Chem.* **2005**, *57*, 173–237.

[15] a) G. Tallec, P. H. Fries, D. Imbert, M. Mazzanti, *Inorg. Chem.* **2011**, *50*, 7943–7945; b) G. Tallec, D. Imbert, P. H. Fries, M. Mazzanti, *Dalton Trans.* **2010**, *39*, 9490–9492; c) F. Caillé, C. S. Bonnet, F. Buron, S. Villette, L. Helm, S. Petoud, F. Suzenet, É. Tóth, *Inorg. Chem.* **2012**, *51*, 2522–2532; d) C. S. Bonnet, F. Buron, F. Caillé, C. M. Shade, B. Drahos, L. Pellegatti, J. Zhang, S. Villette, L. Helm, C. Pichon, F. Suzenet, S. Petoud, É. Tóth, *Chem. Eur. J.* **2012**, *18*, 1419–1431; e) G. Dehaen, S. V. Eliseeva, K. Kimpe, S. Laurent, L. Vander Elst, R. N. Muller, W. Dehaen, K. Binnemans, T. N. Parac-Vogt, *Chem. Eur. J.* **2012**, *18*, 293–302; f) M. P. Placidi, J. Engelmann, L. S. Natrajan, N. K. Logothetis, G. Angelovski, *Chem. Commun.* **2011**, *47*, 11534–11536; g) C. S. Bonnet, É. Tóth, *C. R. Chim.* **2010**, *13*, 700–714; h) S. Laurent, L. Vander Elst, M. Wautier, C. Galaup, R. N. Muller, C. Picard, *Bioorg. Med. Chem. Lett.* **2007**, *17*, 6230–6233.

[16] L. Pellegatti, J. Zhang, B. Drahos, S. Villette, F. Suzenet, G. Guillaumet, S. Petoud, É. Tóth, *Chem. Commun.* **2008**, 6591–6593.

[17] a) W.-S. Li, J. Luo, F. Jiang, Z.-N. Chen, *Dalton Trans.* **2012**, *41*, 9405–9410; b) J. E. Jones, A. J. Amoroso, I. M. Dorin, G. Parigi, B. D. Ward, N. J. Buurma, S. J. Pope, *Chem. Commun.* **2011**, *47*, 3374–3376.

[18] a) L. Frullano, T. J. Meade, *J. Biol. Inorg. Chem.* **2007**, *12*, 939–949; b) F. Lux, S. Roux, P. Perriat, O. Tillement, *Curr. Inorg. Chem.* **2011**, *1*, 117–129.

[19] A. Nonat, M. Regueiro-Figueroa, D. Esteban-Gomez, A. de Blas, T. Rodriguez-Blas, C. Platas-Iglesias, L. J. Charbonnière, *Chem. Eur. J.* **2012**, *18*, 8163–8173.

[20] L. J. Charbonnière, S. Faulkner, C. Platas-Iglesias, M. Regueiro-Figueroa, A. Nonat, T. Rodríguez-Blas, A. de Blas, W. S. Perry, M. Tropiano, *Dalton Trans.* **2013**, *42*, 3667–3681.

[21] a) M. Mato-Iglesias, T. Rodriguez-Blas, C. Platas-Iglesias, M. Starck, P. Kadjane, R. Ziessel, L. J. Charbonnière, *Inorg. Chem.* **2009**, *48*, 1507–1518; b) N. N. Katia, A. Lecointre, M. Regueiro-Figueroa, C. Platas-Iglesias, L. J. Charbonnière, *Inorg. Chem.* **2011**, *50*, 1689–1697.

[22] a) E. Brunet, O. Juanes, R. Sedano, J.-C. Rodriguez-Ubis, *Photochem. Photobiol. Sci.* **2002**, *1*, 613–618; b) M. J. Remuinan, H. Roman, M. T. Alonso, J. C. Rodriguez-Ubis, *J. Chem. Soc. Perkin Trans. 2* **1993**, 1099–1102.

[23] M. Starck, P. Kadjane, E. Bois, B. Darbouret, A. Incamps, R. Ziessel, L. J. Charbonnière, *Chem. Eur. J.* **2011**, *17*, 9164–9179.

[24] A. Barge, L. Tei, D. Upadhyaya, F. Fedeli, L. Beltrami, R. Stefania, S. Aime, G. Cravotto, *Org. Biomol. Chem.* **2008**, *6*, 1176–1184.

[25] M. Regueiro-Figueroa, D. Esteban-Gomez, A. de Blas, T. Rodriguez-Blas, C. Platas-Iglesias, *Eur. J. Inorg. Chem.* **2010**, 3586–3595.

[26] a) L. S. Natrajan, A. J. L. Villaraza, A. M. Kenwright, S. Faulkner, *Chem. Commun.* **2009**, 6020–6022; b) M. Main, M. M. Meloni, M. Jauregui, D. Sykes, S. Faulkner, A. M. Kenwright, J. S. Snaith, *Chem. Commun.* **2008**, 5212–5214.

[27] J.-C. G. Bünzli, *Chem. Rev.* **2010**, *110*, 2729–2755.

[28] A. Beeby, I. M. Clarkson, R. S. Dickins, S. Faulkner, D. Parker, L. Royle, A. S. de Sousa, J. A. G. Williams, M. Woods, *J. Chem. Soc. Perkin Trans. 2* **1999**, 493–503.

[29] H. Ishida, S. Tobita, Y. Hasegawa, R. Katoh, K. Noaki, *Coord. Chem. Rev.* **2010**, *254*, 2449–2458.

[30] J. Olmsted III, *J. Phys. Chem.* **1979**, *83*, 2581–2584.

[31] M. Botta, S. Aime, A. Barge, G. Bobba, R. S. Dickins, D. Parker, E. Terreno, *Chem. Eur. J.* **2003**, *9*, 2102–2109.

[32] S. Aime, M. Botta, S. G. Crich, G. Giovenzana, R. Pagliarin, M. Sisti, E. Terreno, *Magn. Reson. Chem.* **1998**, *36*, S200–S208.

[33] a) N. Bloembergen, *J. Chem. Phys.* **1957**, *27*, 572–573; b) I. Solomon, *Phys. Rev.* **1955**, *99*, 559–565; c) N. Bloembergen, L. O. Morgan, *J. Chem. Phys.* **1961**, *34*, 842–850.

[34] J. H. Freed, *J. Chem. Phys.* **1978**, *68*, 4034–4037.

[35] A. Roca-Sabio, C. S. Bonet, M. Mato-Iglesias, D. Esteban-Gomez, E. Toth, A. de Blas, T. Rodriguez-Blas, C. Platas-Iglesias, *Inorg. Chem.* **2012**, *51*, 10893–10903.

[36] D. H. Powell, O. M. Ni Dhubhghaill, D. Purbanz, L. Helm, Y. S. Lebedev, W. Schlaepfer, A. E. Merbach, *J. Am. Chem. Soc.* **1996**, *118*, 9333–9346.

[37] D. Esteban-Gómez, A. de Blas, T. Rodriguez-Blas, L. Helm, C. Platas-Iglesias, *ChemPhysChem* **2012**, *13*, 3640–3650.

[38] a) A. Mishra, P. Fouskova, G. Angelovski, E. Balogh, A. K. Mishra, N. K. Logothetis, E. Toth, *Inorg. Chem.* **2008**, *47*, 1370–1381; b) J. Costa, E. Toth, L. Helm, A. E. Merbach, *Inorg. Chem.* **2005**, *44*, 4747–4755.

[39] W.-H. Li, G. Parigi, M. Fragai, C. Luchinat, T. J. Meade, *Inorg. Chem.* **2002**, *41*, 4018–4024.

[40] E. Tóth, O. M. Ni Dhubhghaill, G. Besson, L. Helm, A. E. Merbach, *Magn. Reson. Chem.* **1999**, *37*, 701–708.

[41] a) S. Laus, R. Ruloff, E. Toth, A. E. Merbach, *Chem. Eur. J.* **2003**, *9*, 3555–3566; b) J. Kotek, P. Lebduskova, P. Hermann, L. Vander Elst, R. N. Muller, C. F. G. C. Geraldes, T. Maschmeyer, I. Lukes, J. A. Peters, *Chem. Eur. J.* **2003**, *9*, 5899–5915; c) E. Balogh, M. Mato-Iglesias, C. Platas-Iglesias, E. Toth, K. Djanashvili, J. A. Peters, A. de Blas, T. Rodriguez-Blas, *Inorg. Chem.* **2006**, *45*, 8719–8728.

[42] P. Caravan, C. T. Farrar, L. Frullano, R. Uppal, *Contrast Media Mol. Imaging* **2009**, *4*, 89–100.

[43] a) P. Caravan, *Chem. Soc. Rev.* **2006**, *35*, 512–523; b) M. Botta, L. Tei, *Eur. J. Inorg. Chem.* **2012**, 1945–1960.

[44] a) N. J. J. Johnson, W. Oakden, G. J. Stanisz, R. S. Prosser, F. C. J. M. van Veggel, *Chem. Mater.* **2011**, *23*, 3714–3722; b) F. Carniato, K. Thangavel, L. Tei, M. Botta, *J. Mater. Chem. B* **2013**, *1*, 2442–2446.

[45] J. Costa, E. Balogh, V. Turcry, R. Tripier, M. Le Baccon, F. Chuburu, H. Handel, L. Helm, E. Toth, A. E. Merbach, *Chem. Eur. J.* **2006**, *12*, 6841–6851.

[46] N. Fatin-Rouge, E. Toth, D. Perret, R. H. Backer, A. E. Merbach, J.-C. G. Bunzli, *J. Am. Chem. Soc.* **2000**, *122*, 10810–10820.

[47] a) M. B. Inoue, M. Inoue, Q. Fernando, *Inorg. Chim. Acta* **1995**, *232*, 203–206; b) S. I. Kang, R. S. Ranganathan, J. E. Emswiler, K. Kumar, J. Z. Gougoutas, M. F. Malley, M. F. Tweedle, *Inorg. Chem.* **1993**, *32*, 2912–2918.

[48] M. Mato-Iglesias, A. Roca-Sabio, Z. Palinkas, D. Esteban-Gomez, C. Platas-Iglesias, E. Toth, A. de Blas, T. Rodriguez-Blas, *Inorg. Chem.* **2008**, *47*, 7840–7851.

[49] M. Jauregui, W. S. Perry, C. Allain, L. R. Vidler, M. C. Willis, A. M. Kenwright, J. S. Snaith, G. J. Stasiuk, M. P. Lowe, S. Faulkner, *Dalton Trans.* **2009**, 6283–6285.

[50] G. A. Crosby, J. N. Demas, *J. Phys. Chem.* **1971**, *75*, 991–1024.

[51] D. M. Corsi, C. Platas-Iglesias, H. van Bekkum, J. A. Peters, *Magn. Reson. Chem.* **2001**, *39*, 723–726.

[52] Gaussian 09, Revision A.02, M. J. Frisch, G. W. Trucks, H. B. Schlegel, G. E. Scuseria, M. A. Robb, J. R. Cheeseman, G. Scalmani, V. Barone, B. Mennucci, G. A. Petersson, H. Nakatsuji, M. Caricato, X. Li, H. P. Hratchian, A. F. Izmaylov, J. Bloino, G. Zheng, J. L. Sonnenberg, M. Hada, M. Ehara, K. Toyota, R. Fukuda, J. Hasegawa, M. Ishida, T. Nakajima, Y. Honda, O. Kitao, H. Nakai, T. Vreven, J. A. Montgomery, Jr., J. E. Peralta, F. Ogliaro, M. Bearpark, J. J. Heyd, E. Brothers, K. N. Kudin, V. N. Staroverov, R. Kobayashi, J. Normand, K. Raghavachari, A. Rendell, J. C. Burant, S. S. Iyengar, J. Tomasi, M. Cossi, N. Rega, J. M. Millam, M. Klene, J. E. Knox, J. B. Cross, V. Bakken, C. Adamo, J. Jaramillo, R. Gomperts, R. E. Stratmann, O. Yazyev, A. J. Austin, R. Cammi, C. Pomelli, J. W. Ochterski, R. L. Martin, K. Morokuma, V. G. Zakrzewski, G. A. Voth, P. Salvador, J. J. Dannenberg, S. Dapprich, A. D. Daniels, Ö. Farkas, J. B. Foresman, J. V. Ortiz, J. Cioslowski, D. J. Fox, Gaussian, Inc. Wallingford CT, **2009**.

[53] M. Dolg, H. Stoll, A. Savin, H. Preuss, *Theor. Chim. Acta* **1989**, *75*, 173–194.

[54] U. Cosentino, A. Villa, D. Pitea, G. Moro, V. Barone, A. Maiocchi, *J. Am. Chem. Soc.* **2002**, *124*, 4901–4909.

[55] a) A. D. Becke, *J. Chem. Phys.* **1993**, *98*, 5648–5652; b) C. Lee, W. Yang, R. G. Parr, *Phys. Rev. B* **1988**, *37*, 785–789.

[i] Supporting information for this article is available online: https://doi.org/10.1002/chem.201301231.